JOURNAL OF GEOPHYSICAL RESEARCH, VOL. 104, NO. D8, PAGES 9151–9167, APRIL 27, 1999

Use of on-line tracers as a diagnostic tool in general circulation model development
2. Transport between the troposphere and stratosphere

D. Rind, J. Lerner,[1] K. Shah,[2] and R. Suozzo[2]

Goddard Institute for Space Studies, Goddard Space Flight Center, New York

Abstract. The effect of altering the vertical resolution of a general circulation model and processes associated with it are used to investigate mixing between the troposphere and stratosphere. Four on-line tracers are employed: chlorofluorocarbon-11 and SF_6 for mixing from the troposphere into the stratosphere, Rn^{222} for vertical mixing within the troposphere, and ^{14}C for mixing from the stratosphere into the troposphere. Four standard models are tested, with varying vertical resolution, gravity wave drag, and location of the model top, and additional subsidiary models are employed to examine specific features. The results show that proper vertical transport between the troposphere and stratosphere in the Goddard Institute for Space Studies models requires lifting the top of the model considerably out of the stratosphere and including gravity wave drag in the lower stratosphere. Increased vertical resolution without these aspects does not improve tropospheric-stratospheric exchange. The transport appears to be driven largely by the residual circulation within the stratosphere; associated Eliassen-Palm flux convergences require both realistic upward propagating energy from the troposphere and realistic pass-through possibilities. A 23-layer version with a top at the mesopause and incorporating gravity wave drag appears to have reasonable stratospheric-tropospheric exchange in terms of both the resulting tracer distributions and atmospheric mass fluxes.

1. Introduction

The continued development of general circulation models (GCMs) has featured an increase in both horizontal and vertical resolution. While the effects of horizontal resolution have been often examined [*Hoke*, 1987; *Boer and Lazare*, 1988; *Rind*, 1988; *Boville*, 1991; *Boyle*, 1993; *Jones et al*., 1997], the effects of vertical resolution have received less scrutiny. Outside of the general impression that finer vertical resolution is better, there is little consensus in the modeling community on what the vertical resolution should be. Models used in the Intergovernmental Panel on Climate Change (*IPCC*) [1992] assessment of climate change generally had between 9 and 12 layers, while models run for the Atmospheric Model Intercomparison Project (AMIP) comparison had between 10 and 20 [*Phillips*, 1994].

Additional questions concern where the vertical resolution should be increased. Again, the prevailing viewpoint is that higher resolution is beneficial in the boundary layer, to allow for simulation of topographic effects and stable atmospheric conditions, and near the tropopause, for the sake of tropospheric-stratospheric exchange. Middle tropospheric improvements may be beneficial, to allow for wave generation consistent with finer horizontal resolution.

Considering exchange with the stratosphere, additional questions arise. Does the location of the model top influence exchange processes with the troposphere? How does the use of gravity wave drag parameterizations affect tracers? How well do regions in the middle and upper stratosphere need to be resolved? These questions are particularly relevant for the models used in the AMIP runs, whose model tops generally vary between 1 and 20 mbar [*Phillips*, 1994] and have a wide variety of gravity wave drag parameterizations (or none at all).

In the first part of this series we examined the effects of model parameterizations on the horizontal and vertical transport within the troposphere. In this paper we concentrate on exchange between the troposphere and stratosphere (a future paper will be concerned with circulation within the stratosphere).

The model and its various perturbations are discussed in the next section. Results for transport from the troposphere into the stratosphere are given in section 3. Tracer transport from the stratosphere into the troposphere is presented in section 4. Brief results concerning the effect of vertical resolution within the troposphere are given for vertical mixing (section 5) and horizontal transport (section 6). A discussion of timing considerations is presented in section 7 along with a general discussion followed by the main conclusions.

2. Model and Experiments

The base version of the GCM used is that described by *Rind and Lerner* [1996] [hereinafter referred to as part I] as the Summer Institute model (SIM). It consists of the Goddard Institute for Space Studies (GISS) GCM run at $4° \times 5°$ resolution with new parameterizations for the boundary layer [*Hartke and Rind*, 1997], convection [*Del Genio and Yao*, 1992], land surface [*Rosenzweig and Abramopolous*, 1997], clouds [*Del Genio et al*., 1995], a fourth-order B grid momentum advection

[1]Also at Science Systems and Applications, New York.
[2]Also at Center for Climate Systems Research, Columbia University, New York.

Paper number 1999JD900006.
0148-0227/99/1999JD900006$09.00

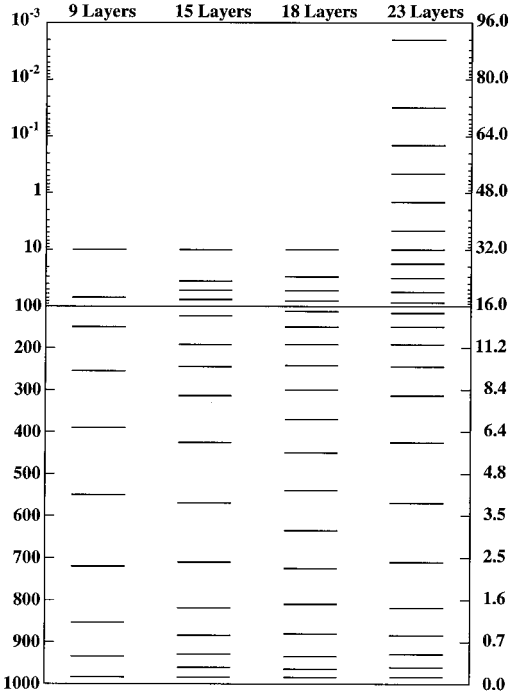

Figure 1. Distribution of model levels in the standard runs. Shown are the layer edges as a function of (left) pressure and (right) altitude.

scheme developed by F. Abramopolous, and a quadratic upstream scheme for heat and moisture advection patterned after that of *Prather* [1986]. The standard model version has 9 layers in the vertical with a model top at 10 mbar and a parameterized drag in the top model layer independent of specific gravity wave sources.

Various versions of this model are used for the tests described below. Each contains all the features noted above, except as indicated. The models tested were: 9L: the standard model but with a second-order closure scheme in the boundary layer [after *Galperin et al*., 1988]; 15L: the standard model except increased vertical resolution plus parameterized gravity wave drag between 82 and 10 mbar; 18L: as in 9L except increased vertical resolution; and 23L: as in 15L except the model top is raised to 0.002 mbar (~85 km) and gravity wave drag extends from 425 mbar to the model top.

In addition to these standard experiments, subsidiary runs were performed to examine certain model characteristics in more detail. In particular, 23LT is similar to 23L except the model top is lowered to 0.4 mbar (~55 km). This and other experiments will be introduced during the presentation of the results.

The chief difference amongst the models is the vertical resolution. Shown in Figure 1 are the levels for the models used. All the higher vertical resolution models have increased layering in the boundary layer and near the tropopause compared to the 9-level version. Only 18L has more layers in the middle troposphere as well. Model 23L has a model top near the mesopause, while the other versions have the top in the middle stratosphere.

Another difference is that two of them (9L and 18L) use a second-order closure boundary layer parameterization. This was done in an attempt to determine whether the impact of the boundary layer vertical resolution is dependent upon a particular physical parameterization. Comparisons will be made with a standard version of the model utilizing the SIM boundary layer, which is a modified Ekman layer [*Hartke and Rind*, 1997]. It turns out that the results are insensitive to this completely different boundary layer formulation, a quite surprising conclusion considering that a previous change in boundary layer parameterization played a dominant role in improving model simulations, as discussed in part I. Apparently, once the deficiencies of the GISS model II boundary layer [*Hansen et al*., 1983] were corrected, additional improvements did not have a significant impact on tracer distributions.

A third major difference involves the gravity wave drag. The 9-layer model utilizes a drag in its top layer that is similar to frictional drag near the surface: a drag coefficient for momentum (C_d) is calculated that depends upon the local Richardson number (hence stability and shear), and this value multiplied by the density and wind squared ($\rho C_d V^2$) provides the drag [*Hansen et al*., 1983]. This formulation is also used in the top layer of 18L. In contrast, 15L and 23L employ parameterized gravity wave drag sources from flow over mountains, convection, and nongeostrophic effects (shear and fronts); the momentum fluxes then propagate vertically and break following the linear saturation theory. A complete description is provided by *Rind et al*. [1988]. At the top of the model all the parameterized wave sources are allowed to break (regardless of the instability criteria). Therefore, in contrast to 9L and 18L, 15L and 23L have gravity wave drag in layers below the top.

Associated with the gravity wave drag on momentum is a vertical diffusion of momentum, as discussed by *Rind et al*. [1988]. However, with the assumption that gravity wave breaking is an adiabatic process and occurs along isentropes and that tracers follow isentropes, in general, the vertical diffusion is not used to alter the tracer distribution (or potential temperature). None of the models contain any other form of explicit vertical diffusion. The use of the quadratic upstream scheme for tracer advection also limits the numerical diffusion in all directions, including the vertical [*Prather*, 1986].

Each model ran for 6 years with four tracers; results are presented for the last 5 years. For chlorofluorocarbon (CFC)-11 and Rn^{222} the nature of the results is well established by the second year. SF_6 results are not quite in equilibrium at this time, although, as will be shown, the results are not significantly altered when the SF_6 simulation is extended out to 10 years (for age of air considerations). For ^{14}C the time-transgressive nature of the output is of interest and will be discussed. As noted in part I, the use of on-line tracers as a standard procedure in model development augments the meteorological parameters usually perused and helps provide information on the validity of model transports not easily deducible otherwise. Off-line analysis in a chemical tracer model (CTM) is also feasible, although the requisite fields must be continually saved and, sometimes, the structure of the CTM altered along with that of the GCM.

3. Transport From the Troposphere Into the Stratosphere

3.1. CFC-11

The basic characteristics of this experiment were discussed in part I. The geographically varying emissions are those designed for the World Climate Research Program (WCRP) model intercomparison [*Prather*, 1992; *Prather and Remsberg*,

Table 1. Percentage Rate of Increase of CFC-11 in the Different Models, Along With the Vertical Transport Through the 100 mbar Level and the Stratospheric Chemical Loss (5 Year Average)

	9L	15L	18L	23L	23LT	Observation
Rate of increase, %	3.79	3.07	1.67	3.86		4.0*
Transport through 100 mbar, kg s^{-1}	3.6	4.3	6.9	3.0		
Chemical loss, kg s^{-1}	2.9	4.3	6.9	3.0		
Lifetime, years	65.6	42.7	25.4	57.6		35–50
E-P flux conversion						
90–10 mbar (10^{16} J)	1413	1211	1270	986	1034	
10–0.5 mbar				(1029)	(1449)	
Stratospheric gravity wave drag						
90–10 mbar (10^{16} J)	1013	602	820	397	407	
10–0.5 mbar				(−69)	(−403)	
Tropospheric eddy energy (10^{17} J)	2868	3004	3496	2317	2369	
Eddy energy at 200 mbar (J m^{-2})	132	132	186	94	100	
Eddy vertical transport of geopotential through 100 mbar	102	84	119	74	80	

*During the period 1980–1989.

1993]. As expected, Northern Hemisphere industrial countries dominate the source. The sink is due to transport into the stratosphere. In 9L the stratospheric loss is proportional to the mass of CFC-11 in the top layer (the only true stratospheric layer). In all the other model versions the stratospheric loss is calculated from the CFC-11 stratospheric chemistry sink defined by M. Prather, which varies somewhat with the vertical resolution used. As most of this sink occurs between 20 and 90 mbar, the location of the model top is not important.

Since the source is in the troposphere and the loss is in the stratosphere the rate of growth of CFC-11 is indicative of the magnitude of transport into the stratosphere. The percentage rate of increase for the different models is given in Table 1.

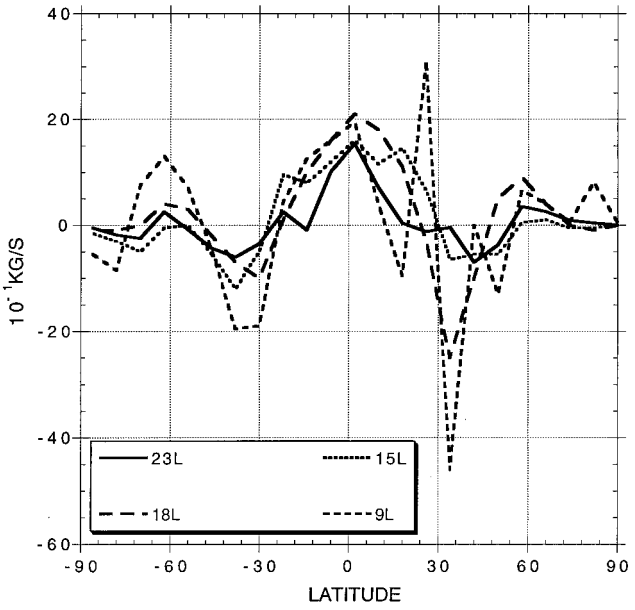

Figure 2. Annual average vertical transport of CFC-11 through the 100 mbar level. Results are 5 year averages for each model, unless otherwise stated. As defined here and throughout the paper, the vertical transport is the model's calculated vertical velocity (the sum of mean circulation plus eddy components) multiplied by the species concentration; it does not include convective mixing (negligible by comparison at this level).

The 18L model has the slowest rate of growth (and hence is furthest from the observations), while the 9L and 23L are closest to the observations. The 9L and 23L also have the longest lifetimes; the estimated observed lifetime for CFC-11 is thought to lie somewhere in the range of 35–50 years [*Kaye et al*., 1994]. The rate of growth is related to the stratospheric chemical loss (the only loss process), which in turn is related to the transport of material through 100 mbar, the tropical tropopause level; transport into the stratosphere occurs basically between 10°N and 10°S on the annual average in all the models. Except for the 9L model, in which a total loss was prescribed and proportioned according to concentration, the chemical loss in the other experiments equals the transport through 100 mbar. (From the vertical transport values it appears as if the 9L run would have had a slightly smaller rate of increase had it used a chemical, rather than prescribed, loss). Therefore the difference among the models is related to the different net transport from the troposphere into the stratosphere.

Shown in Figure 2 is the vertical transport through 100 mbar in the different model simulations. In basically all the models, CFC-11 transport is upward at low latitudes and also from 45° to 70° latitude, while it is downward from 30° to 45° latitude. The 9L model has exaggerated values, while the 18L produces very smooth patterns. Compared with the 23L model, all the other models have greater transport upward through 100 mbar between 20°N and 20°S, with somewhat greater downward transport from 30° to 45°.

What accounts for the transport differences among the models? More rapid transport through the tropopause could result from more rapid transport up from lower levels. Annual vertical transports between 12°N and 12°S within the troposphere are given in Figure 3. While there are differences below 200 mbar (23L and 15L have the largest Hadley Circulation intensity in the troposphere, as discussed further in section 5), there is no correlation between transport (or convergence) through the 200 mbar level, or any level below, and the transport through the tropical tropopause near 100 mbar. Convection produces negligible CFC-11 mass transport compared to the large-scale circulation in the tropical upper troposphere.

Therefore the difference relates primarily to the transport near the tropopause itself. Transport through the tropical tropopause is thought to be part of the large-scale circulation

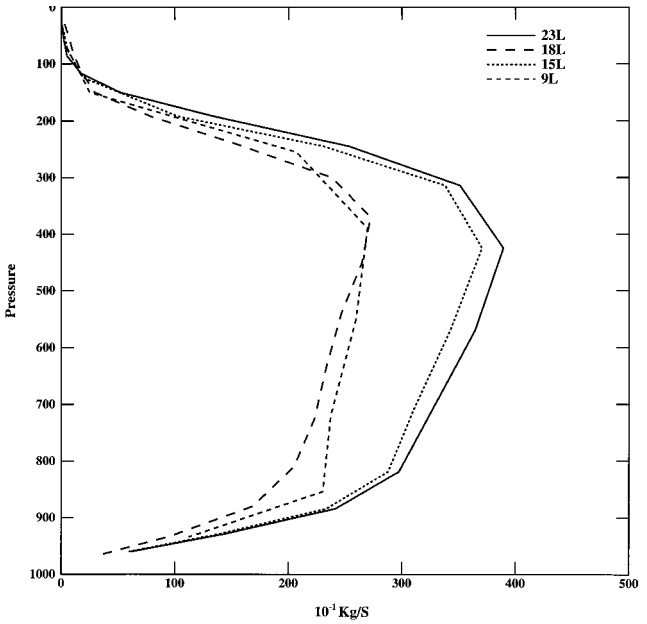

Figure 3. Vertical transport of CFC-11 in the tropics (12°N–12°S).

in the stratosphere [*Holton et al*., 1995]. *Holton et al*. [1995] argue that for transport through 100 mbar the value of the circulation in the subtropics may be more important than that at higher latitudes. Therefore a comparison of the subtropical residual circulation mass transport is presented in Figure 4 for the winter season in each hemisphere. The values for 23L are considerably smaller than those for the other models; hence the greater average transport in other models compared to the 23L result is consistent with their greater residual circulation. While observations of this diagnostic are somewhat uncertain, shown for comparison are those generated from UARS data [*Eluszkiewicz et al*., 1997]. In general, 23L is the most realistic of the different GCM runs, with all the other models producing exaggerated values in the lower stratosphere and 18L having the largest. Consistent with this characteristic, 18L has the coldest tropical tropopause temperatures, being 2°C colder than 23L in each season.

The residual circulation is driven by E-P flux and gravity wave drag convergences. Given in Table 1 is the annual average E-P flux convergence for the region between 90 and 10 mbar. Model 23L has the lowest value, consistent with its reduced residual circulation, while 18L has the largest. Also shown are the stratospheric gravity wave drag values. Model 23L again has the lowest value, primarily because in the other models, with their tops at 10 mbar, more drag is needed to counteract its influence in this region. Considering both driving forces, 18L has 1.5 times greater forcing of the residual circulation than 23L. The different transport capabilities from the troposphere to the stratosphere therefore appear to be related to the eddy E-P flux and parameterized gravity wave flux convergences in the low to middle stratosphere.

Observations show peak E-P flux convergence values during winter to be $>3 \times 10^{-5}$ m s^{-2} between the tropopause and 10 mbar [e.g., *Wu et al*., 1987; *Rosenlof and Holton*, 1993]. In 18L, values of 3–4 $\times 10^{-5}$ exist from 35° to 65°N on average in winter at 40 mbar; high values are also found in 15L and 9L. In contrast, no value $>3 \times 10^{-5}$ occurs on average in this height region in 23L.

A rough correspondence exists between the E-P flux convergence in the low to middle stratosphere and eddy energy in the upper troposphere. Also included in Table 1 are the global average tropospheric and 200 mbar eddy energy values for the different models; clearly, 18L has the most energy, and 23L has the least. Dynamical generation of eddy energy is 33% greater in 18L than in 23L. The actual resolution in the upper troposphere is very similar in most of the models, so the difference is not related to that. 23L includes gravity wave drag extending down to 425 mbar, but when in a separate simulation gravity wave drag was not allowed below 100 mbar (23L-GW100), the eddy energy at 200 mbar was only 10–15% larger. However, the 23L model gravity wave drag parameterization affects the stability in the lower stratosphere. Shown in Figure 5 is the zonal average deviation from observed microwave sounding unit (MSU) temperatures of the different models for channel 4 (peak weighting at ~80 mbar), channel 3r (280 mbar), and channel 2 (600 mbar), derived from a microwave radiance postprocessor used with the GCM [*Shah and Rind*, 1995]. Note that 18L has the coldest (and worst) temperatures in the extratropics, with therefore the lowest vertical stability, and 23L has the warmest (and best), with greater vertical stability. Greater stability will inhibit eddy energy production. Also, with greater eddy energy, there is a greater eddy flux of geopotential energy into the stratosphere (Table 1).

Model 15L has a similar gravity wave drag parameterization to 23L, yet it has lower stability and more eddy energy. Two effects are involved: 23L starts its stratospheric drag in the upper troposphere, so some parameterized breaking is occurring prior to reaching 90 mbar, while 15L begins its drag at 90 mbar. In addition, 15L allows all the parameterized waves to break at the model top, which puts substantial drag in this region. To estimate which effect is most important, we can

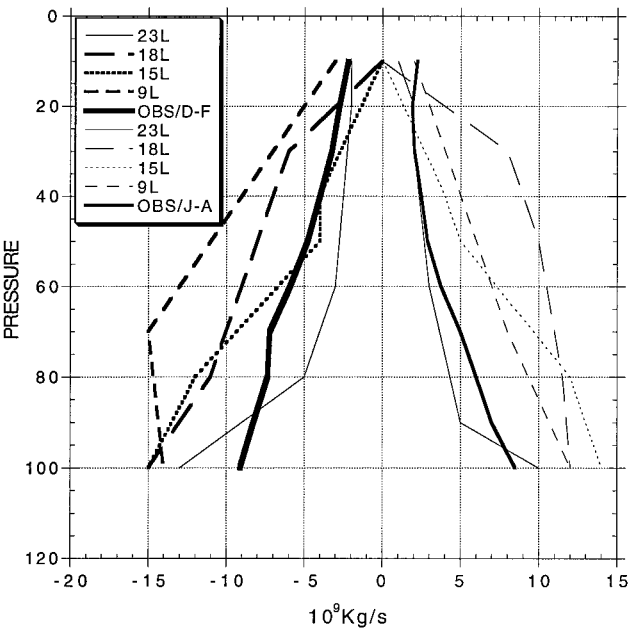

Figure 4. Subtropical residual circulation values for December–February in the Northern Hemisphere (negative values) and June–August in the Southern Hemisphere (positive values). Observations are after *Eluskiewicz et al*. [1997].

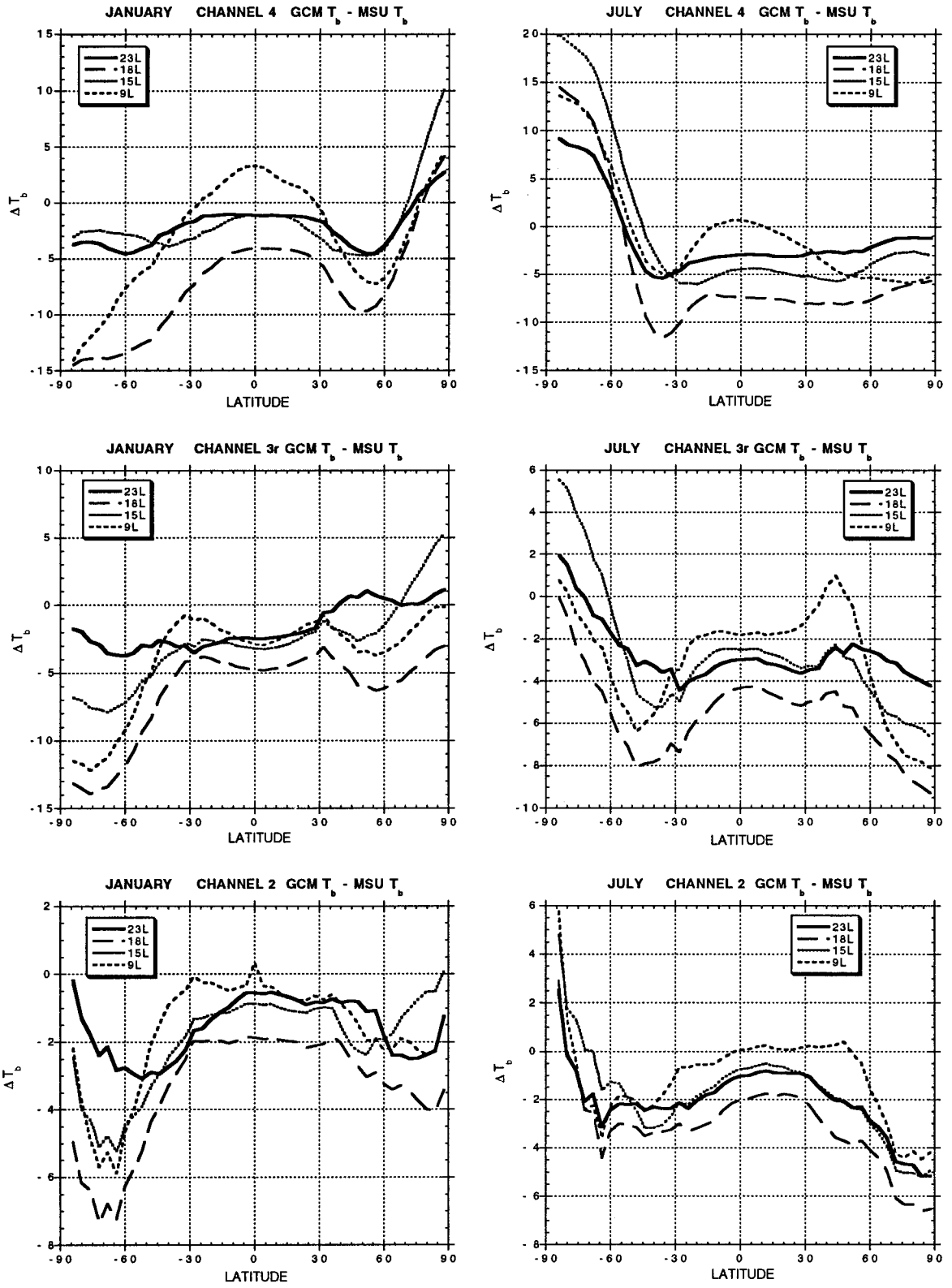

Figure 5. Comparison of general circulation model (GCM) and microwave sounding unit (MSU) weighted temperatures for lower stratosphere channel 4 (mean pressure 80 mbar), upper troposphere channel 3r (mean pressure 280 mbar), and middle troposphere channel 2 (mean pressure 600 mbar). Given are the zonal average differences between the model values calculated with an off-line microwave radiation processor and observations for (left) January and (right) July. Channel 3r values are modified as by *Shah and Rind* [1998].

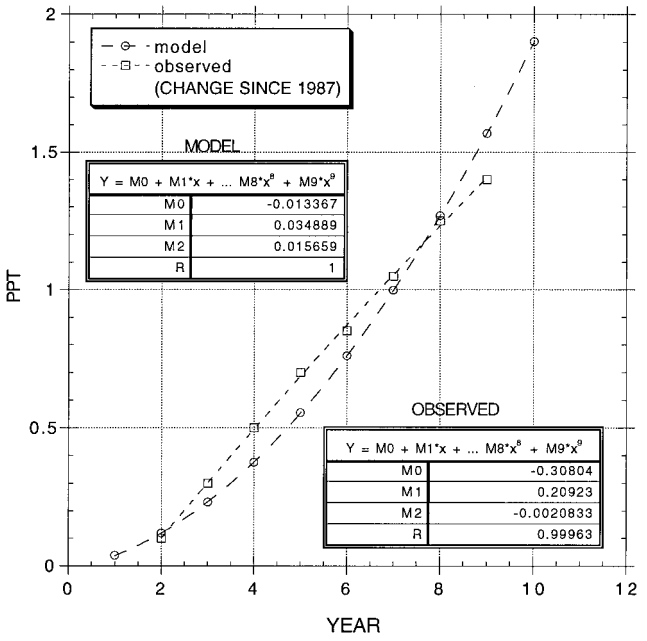

Figure 6. SF_6 in the lowest model layer (results are similar in all models) and observed values minus their 1987 value [from *Geller et al*., 1997]. Also shown are the equations for line fits of the two curves.

refer to the results from 23L-GW100, in which drag was not allowed to begin below 100 mbar. The stratospheric drag went up by ~20%, two fifths of the difference with 15L shown in Table 1. As noted above, removing the drag from the upper troposphere increased the eddy energy there by 10–15%, while the residual circulation in the lower stratosphere increased by up to 20%. While this does not explain most of the difference between 23L and the other models, allowing the drag to start in the upper troposphere does have some effect.

To investigate how far above 10 mbar the top has to be lifted to minimize its effect in the lower stratosphere, another run was made, with the top raised to 0.46 mbar (~55 km) by adding 8 more layers to L15, all above 200 mbar (23LT, for "lower top"). The gravity wave drag reverted back to the values typical of 23L in the middle stratosphere (Table 1), as expected from the discussion above. The E-P flux convergence below 10 mbar was also similar in this region. However, between 10 and 0.46 mbar (the top of this model), the E-P flux convergence (value in parentheses) is 50% greater in 23LT than for the same levels in 23L because of the influence of the top of the model. The gravity wave drag was also enhanced as it acted upon strong winds that are further strengthened by the presence of the model top (the global negative values are because of the effect on tropical east winds). These effects result in a residual circulation increase of some 20% between 100 and 10 mbar and increases of 100% in the upper stratosphere. The direct effect of this intermediate model top position and its "downward control" [*Haynes et al*., 1991] on troposphere-stratosphere exchange will be examined in the sections devoted to SF_6 and ^{14}C. Model 23LT has stability values only slightly worse than 23L, and therefore the tropospheric eddy energy and vertical fluxes through 100 mbar are similar (Table 1).

In a final experiment, with the top of the model at the mesopause the gravity wave drag was removed from the troposphere and stratosphere entirely (23L; no gravity waves (GW)). Tropospheric eddy energy went up by 30%, and E-P flux convergences approaching those in 18L occurred at 10 mbar. Both a high top and gravity wave drag appear to be necessary in this model to minimize the driving forces for the residual circulation.

The eddy energy in 18L is most realistic in total amount, with values close to those given by *Oort* [1983], and its ratio in winter of 200/950 mbar values is also the most realistic (5.9 compared with the observed value of 7.6). This would seem to produce a paradox since 18L is also the worst model for tropospheric-stratospheric exchange. However, there is too much transient energy relative to stationary energy (3.8 compared to 2.9 in the observations), and the linear slope as a function of wavenumber is too small (−0.6 compared to the observed value of −1.2), indicating the longwave energy is deficient. None of the other models do better in any of these respects. Were the planetary longwave energy to be greater and the top of the model absent, planetary waves would more easily propagate through the lower stratosphere and induce less of a residual circulation.

3.2. SF_6

In this experiment a source for SF_6 was input uniformly into the lowest model layer from 20° to 60°N. The distribution differs from that used for CFC-11, which employed a geographical variation related to power consumption and included a small Southern Hemisphere component not present in the SF_6 source we used. The source started at 0.8 Gg yr^{-1}, and it increased 0.8 Gg yr^{-1} until after 10 years it reached 8 Gg yr^{-1}. In comparison, the observed release at the beginning of 1996 was estimated at close to 6 Gg yr^{-1} [*Geller et al*., 1997].

The resulting Northern Hemisphere concentration in the lowest model layer as a function of year is given in Figure 6 along with equations for the curve fit. Also shown is the observed increase, subtracting out the 1987 value [*Geller et al*., 1997] (the model started from zero initial conditions). The model fits a second-order polynomial perfectly, as would be expected from the source increase; observed values are somewhat more linear, but overall, the comparison is sufficient for the current purposes. As noted by *Geller et al*. [1997], the overall increase of SF_6 is best described by a quadratic fit.

The transport through 100 mbar is given in Table 2 along with the ratio of concentration above/below the tropopause. In this paper the tropopause is defined as ~100 mbar in the tropics, while it is ~200 mbar in midlatitudes and 300 mbar in high latitudes; in the extratropics these locations occur close to the 2×10^{-6} m^2 s^{-1} K kg^{-1} value of potential vorticity.

Table 2. SF_6 Tropospheric-Stratospheric Transfer

	9L	15L	18L	23L	23LT	Observations*
Ratio of stratospheric-tropospheric concentrations, %	31.7	24.6	23.6	19.7	22.7	~20.2
Transport through 100 mbar (10^{-2} kg s^{-1})	7.4	6.7	7.5	3.6	6.4	

**Geller et al*. [1997].

Observed values are from *Geller et al*. [1997] (the "f" factor in that paper), although a stratospheric-wide inventory is not available. Again, the 23L values look most realistic, with less transport through 100 mbar and less concentration in the stratosphere than for the other models. The explanation for these differences is similar to that given above for CFC-11, except that now the 9L run does not have specified stratospheric loss rates to produce more realistic ratios.

Another way for tracers to be transported into the stratosphere is via exchange between the tropical upper troposphere and the "lowermost" extratropical stratosphere via horizontal fluxes. (*Holton et al*. [1995, p. 407] call the "lowermost stratosphere" the region where isentropic surfaces span the tropopause".) An estimate of this effect can be obtained by calculating the transport through 30° latitude between 300 and 100 mbar. Only in the 15L model is this effect of any importance, and for the yearly average it results in net transport into the troposphere for SF_6. For CFC-11 the effect is somewhat larger, although in no case does it exceed 25% of the direct vertical transport for either tracer.

In this experiment the SF_6 source was put in uniformly over the latitude band and only in the Northern Hemisphere; what difference would it make if the source were restricted to land and a Southern Hemisphere component added? In addition, the experiments were run for 6 years; how does the ratio vary over time, and how would it be altered if the models were run long enough to achieve equilibrium? These questions were tested in separate experiments with 9L; the results are shown in Figure 7 as the ratio above and below the tropopause. The stratosphere/troposphere ratio does vary with time; the result as the model approaches equilibrium is ~10% higher than the average for years 2–6. The different source distributions make little difference, however.

The effect of the intermediate model top (23LT) on SF_6 transport into the stratosphere is also given in Table 2. In terms of both the ratio above and below the tropopause and the flux through 100 mbar, it is generally similar to 15L; hence lifting the model top by 20 km had no beneficial effect on exchange from the troposphere into the stratosphere.

SF_6 has recently been employed to calculate the age of stratospheric air [e.g., *Hall and Plumb*, 1994; *Patra et al*., 1997; *Volk et al*., 1997; *Waugh et al*., 1997]. Our interest in this paper is in troposphere-stratosphere exchange and not the stratospheric circulation per se (which is the focus of the next paper in this series). Nevertheless, since the magnitude of the circulation originating in the low to middle stratosphere appears to be critical for troposphere-stratosphere exchange the diagnostic is relevant for this study as well.

The age of air is calculated as a lag between the concentration at any level and the global first-layer concentration. As shown in Figure 6, the modeled SF_6 does not represent a purely linear growth. *Volk et al*. [1997] note that the nonlinearity can lead to an underestimation of the age of air by up to 0.5 years for ages of 3–6 years when this simple lag calculation is employed.

For the sake of this calculation the model runs were extended to 10 years duration. The age of air from the different models compared with observations (as by *Waugh et al*. [1997]) is shown in Figure 8. As Waugh et al. did for the middle atmosphere community climate model 2 (MACCM2) winds in a CTM, we show the spread of the age of air from all (72) longitudes for the different altitudes. The spread is indicative of the synoptic distribution of potential vorticity features; in extratropical regions of higher pressure (lower potential vorticity), tropical air can most easily penetrate, producing higher concentrations of SF_6 (coming up through the tropical tropopause) and younger ages of air. In contrast, older ages are found in the polar vortex region.

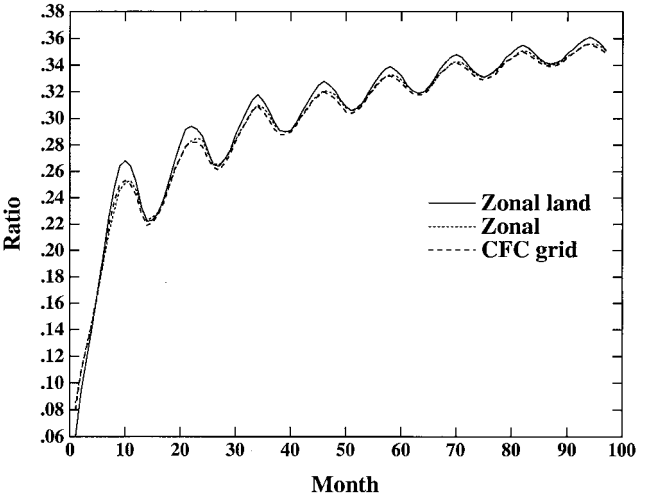

Figure 7. SF_6 stratospheric-tropospheric ratio as a function of month with three different SF_6 sources: zonally uniform over land; zonally uniform; and corresponding to the CFC release grid of *Prather* [1992].

As is obvious from Figure 8, the age of air in 23L is more realistic (i.e., older) than that from the other models, although observations from balloon measurements are sparse and have significant variability. The younger ages are associated with the more vigorous upwelling and stratospheric circulation intensity in the other models. In absolute terms, even 23L produces air that is somewhat too young compared with these observations; the 23L values are similar to those produced by the MACCM2 [*Waugh et al*., 1997].

Not shown in Figure 8 are the results for 23LT, which only ran for 6 years. However, a comparison can be made between the age of air in that simulation and the values from the other runs at an equivalent time. The comparison shows that below 20 km, 23L had mean ages greater than 23LT by ~80%, while from 20 to 35 km its mean ages were greater than 23LT by ~33%. Model 23LT mean age values were quite similar to 15L, so the correspondence visible in Table 2 extends throughout the lower and middle stratosphere. Again, raising the top by 20 km had no beneficial impact as long as the top remained near the stratopause. The mean ages in 23L were some 280% longer than in 18L throughout the lower and middle stratosphere.

4. Transport From the Stratosphere Into the Troposphere

To test the various model transports from the stratosphere down into the troposphere, bomb-produced ^{14}C is used. The initial conditions for the release are from *Johnston* [1989] for October 1963, and the lower boundary is varied as in the following prescription [see also *Prather and Remsberg*, 1993]:

$$\text{Northern Hemisphere } {}^{14}\text{C} = 73.0 - 0.27823t$$

$$- 3.45648\text{E} - 3t^2 + 4.21159\text{E} - 5t^3$$

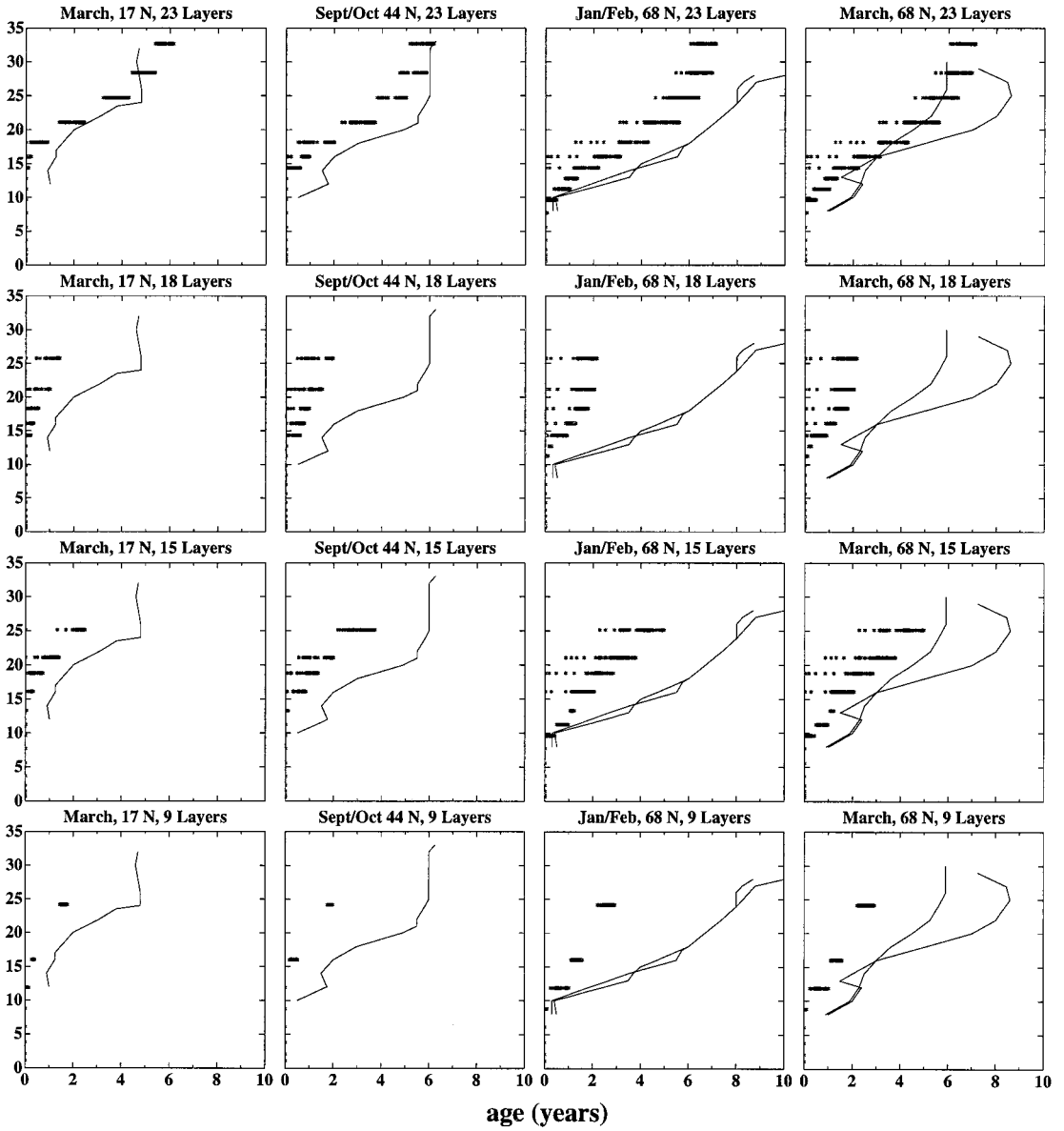

Figure 8. SF_6 age of air for the different models compared with observations as shown by *Waugh et al.* [1997]. Model data points represent the ages at different longitudes.

Southern Hemisphere $^{14}C = 44.5 + 1.02535t$

$$- 2.13565E - 2t^2 + 8.61853E - 5t^3$$

where t is months after October 1963 and the units are 10^5 molecules $^{14}CO_2\ g^{-1}$ of air. At the upper model boundary the flux is set to 0.

Shown in Figure 9 for the different models are (a) the total atmospheric loading of ^{14}C, (c) the stratospheric loading, (b) the tropospheric loading, and (d) the stratosphere/troposphere ratio. The 23L model has the greatest stratospheric loading, the highest stratosphere/troposphere ratio, and the greatest total atmospheric ^{14}C. Model 18L has the lowest values of each of those but has the highest tropospheric loading. Following the procedure given by *Prather and Remsberg* [1993], we calculate the residence time by fitting a least mean square line to the natural logarithm of the concentration as a function of time. The linear regression relationship, correlation coefficient, and residence time for the different models are given in Table 3. These residence times apply for the time period October 1963 through October 1965.

For comparison the residence times given by *Prather and Remsberg* [1993], the average of 12 models for October 1963 through July 1966, was 3.0 years. The range in those models was from 2.3 to 4.1 years. Therefore the 23L model has a longer residence time than any of the previous models (and the values tend to increase with duration, so it would be longer still if calculated through July 1966). The other model results shown in Table 3 fall into the general range given by *Prather and Remsberg* [1993]; again, the 18L has the smallest residence time, indicating fastest stratosphere-troposphere exchange.

How do the results compare with observations? Profiles of ^{14}C for the different solstice seasons at a variety of latitudes following the release in October 1963, compared with the observations shown by *Prather and Remsberg* [1993], are given in

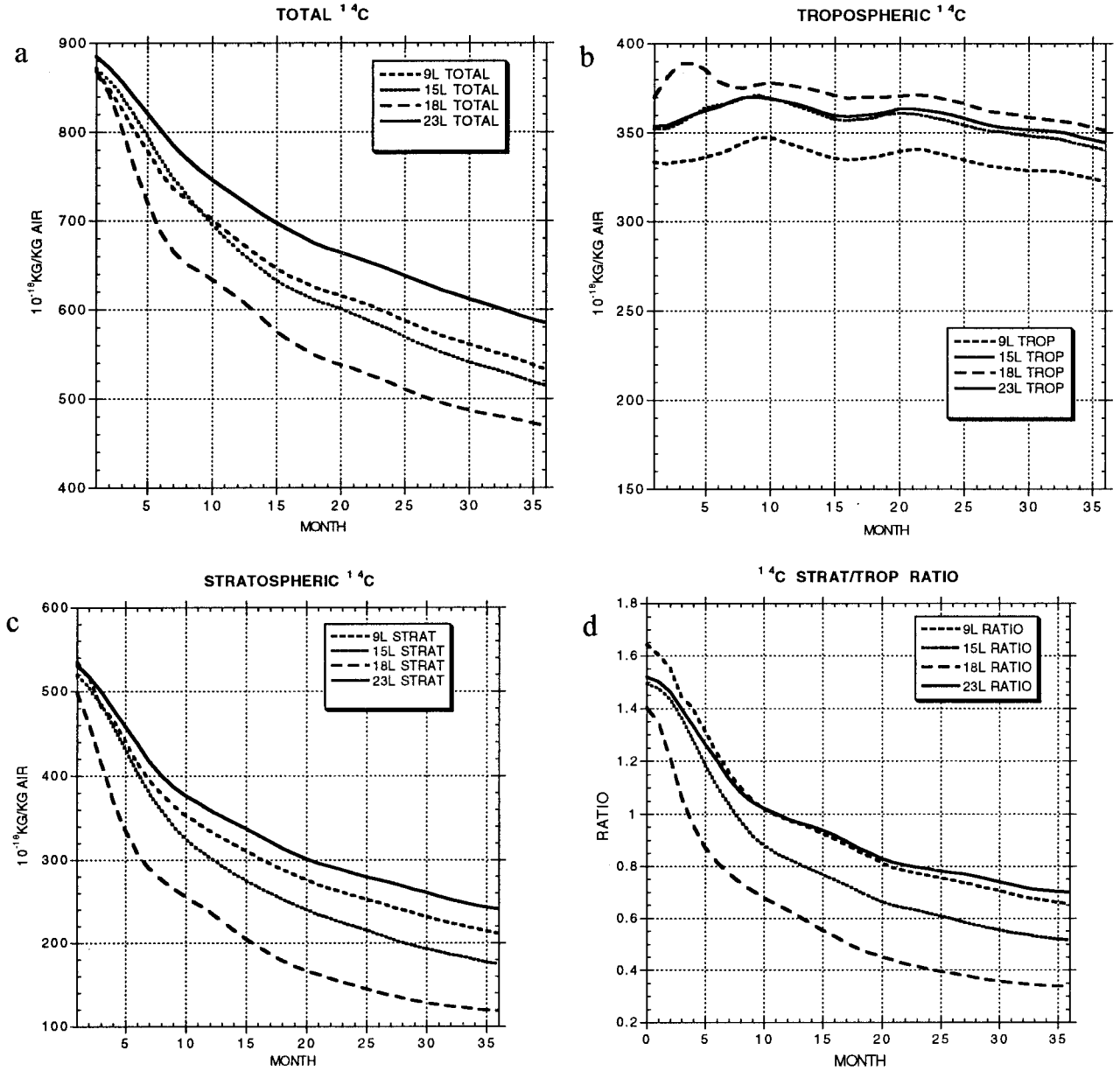

Figure 9. Bomb ^{14}C as a function of time following release; (a) total, (b) tropospheric, (c) stratospheric, and (d) the stratosphere/troposphere ratio (lower right).

Figure 10. As is apparent in Figure 10, the 23L model is clearly better than the versions that have a top at 10 mbar. Its primary deficiency may be an excessive transport upward at lower mid-latitudes, an effect which will be discussed in more detail in part III of this series on the stratospheric circulation. Overall, the 18L model is the least successful. Hence the longer the residence time, the better the model.

Table 3. Stratospheric ^{14}C Residence Time and Associated Linear Regression Statistics With the Different Models

Run	(ln concentration) = m (month) + b	Correlation Coefficient	Residence Time, years
9L	$m = -0.0226$ $b = 6.11$	0.93	3.7
15L	$m = -0.0281$ $b = 6.09$	0.94	3.0
18L	$m = -0.0367$ $b = 5.94$	0.95	2.3
23L	$m = -0.0193$ $b = 6.13$	0.90	4.3
23LT	$m = -0.0216$ $b = 6.10$	0.92	3.8

The ratio of calculated to observed ^{14}C over the 28 months of this experiment averaged 0.83 at 31°N and 20 km and 0.97 at 70°N and 16 km. The other models shown by *Prather and Remsberg* [1993] have their average over this time period ranging from 0.36 to 1.23 at 30°N and 0.56 to 1.36 at 70°N. *Prather and Remsberg* [1993] noted that the three-dimensional (3-D) models tended to underestimate strongly the residence time of ^{14}C in the stratosphere. In that respect the 23L results are better than any of the 3-D models that participated in the first models and measurements exercise.

Where is the transport out of the stratosphere occurring, and how/why does it differ among the different models? Shown in Figure 11 are the vertical transports of ^{14}C through 150

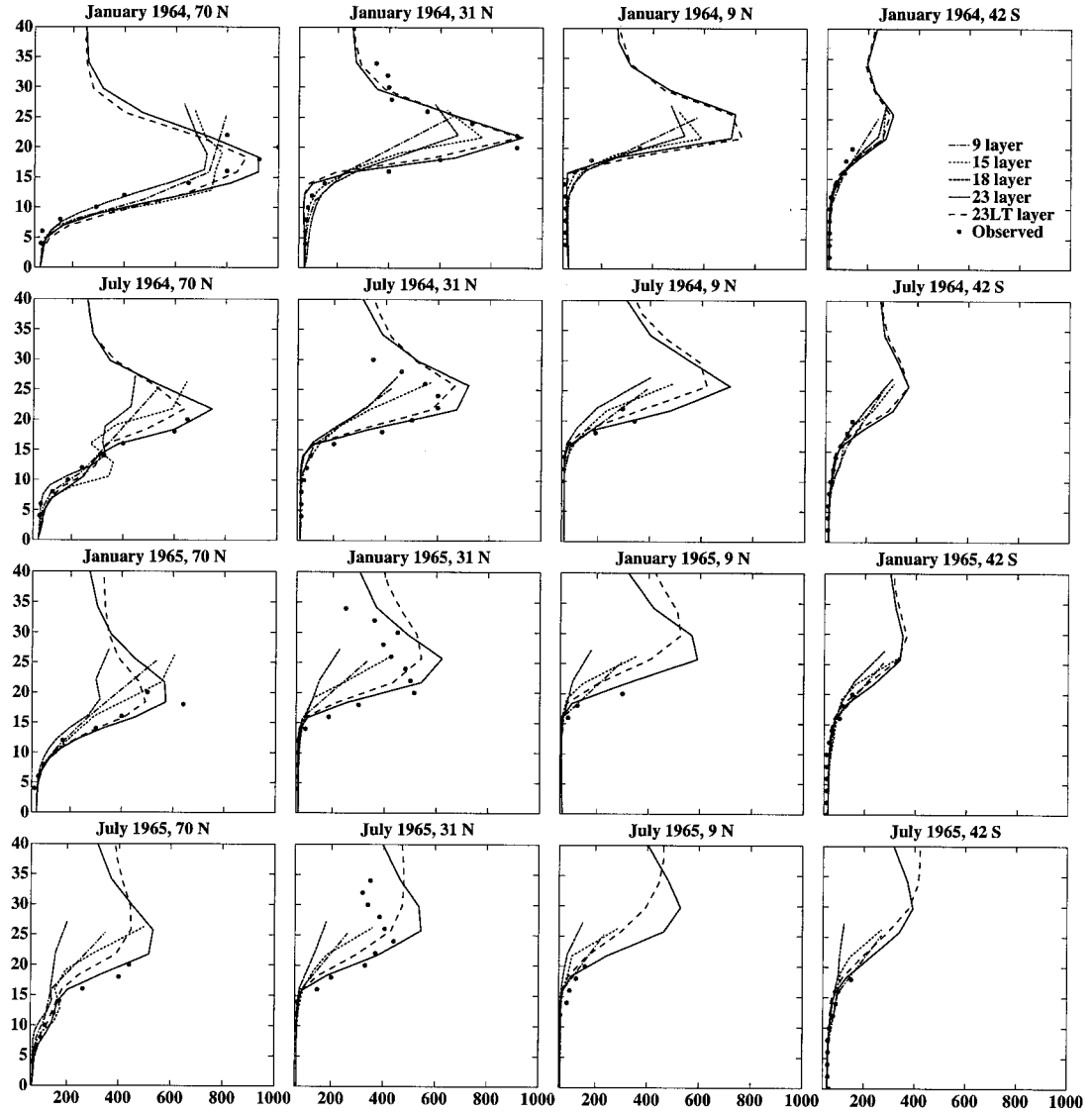

Figure 10. Observed and modeled profiles of ^{14}C (observations as shown by *Prather and Remsberg* [1993]).

mbar in 4 different months. Downward transports generally occur in all models at midlatitudes, especially just poleward of 30°N. The excessive 18L transports occur primarily in winter. Model 9L also has some large downward transports but in addition has some greater upward transports as well. Model 23L appears conservative in all months.

The explanation for these differences is consistent with that presented earlier for upward transports: the residual circulation driven by E-P flux convergences in the stratosphere, with the effect reaching its maximum in Northern Hemisphere winter. Actual transport into the troposphere from the lowermost stratosphere is facilitated in the real world by tropopause folding, cutoff cyclones, etc., phenomena associated with midlatitude eddy energy. As noted previously, 18L has much more eddy energy than 23L, and this is especially true in the upper troposphere, where during Northern Hemisphere winter, values are twice as large. Eddy downward transports of ^{14}C are somewhat larger at these levels in 18L, but the differences are small relative to the differences in eddy energy. *Holton et al.* [1995] show examples indicating that weaker cutoff cyclones sometimes produce greater downward displacement of mixing ratio surfaces than do stronger ones, so a direct relationship with the amount of tropospheric eddy energy should not be expected. Nevertheless, eddies typically account for 20–40% of the downward transport of ^{14}C at 150 mbar in the different models, a nonnegligible contribution. Model 23L has both the weakest stratospheric circulation and the weakest upper tropospheric eddies.

Also shown in Table 3 and Figure 10 are results for 23LT, the model with its top at 55 km. Lowering the top degrades the model's performance relative to 23L (despite there being greater vertical resolution in the stratosphere in 23LT, although not near the tropopause), with a shorter residence time and less accurate match with observations. In this case, however, 23LT is more successful than the 15L results with its reduced vertical resolution and lower top.

5. Vertical Mixing Within the Troposphere

Another component of cross-tropopause mixing that might be affected by the vertical resolution is the mixing to altitude within the troposphere. Although differences in this respect

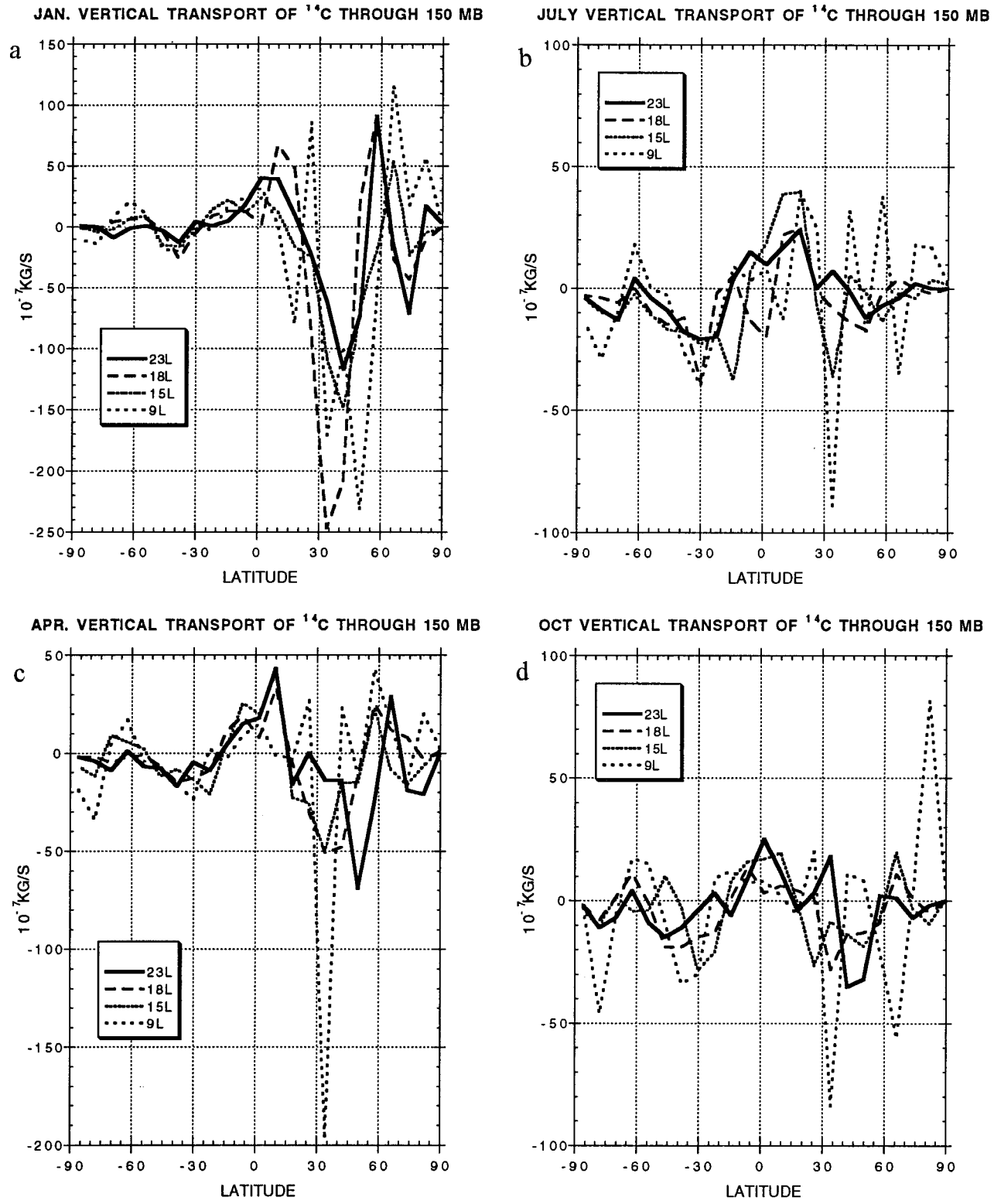

Figure 11. Vertical transport of bomb ^{14}C through the 150 mbar level for (a) January, (c) April, (b) July, and (d) October.

among the models were not shown to be important for CFC-11 fluxes into the stratosphere (Figure 2), seasonal variations in the mixing to the upper troposphere do affect tropospheric-stratospheric exchange, as indicated by the observed seasonal variations of CO_2 within the lower stratosphere [*Boering et al.*, 1994]. (Note that while seasonal variations occur in lower stratospheric water vapor as well [e.g., *McCormick et al.*, 1993; *Mote et al.*, 1995], that may be more a reflection of tropopause temperature variations, even though tropical upper tropospheric water vapor has a similar variation [*Rind et al.*, 1993]).

A good test of tropospheric vertical mixing is provided by using radon as a tracer. With a half life of 3.8 days, radon is basically a test of convection in the model. Since different vertical resolution may alter moist static energy profiles it is possible that convective instability could differ depending on layer thickness and placement.

The radon experiment is the same as that described in part I with the primary emission source being radon decay in soils. Shown in Figure 12a is the global, annual average radon distribution as a function of pressure altitude for the different models. Some differences exist above 400 mbar with the 9L model having slightly higher concentrations and the 23L model being somewhat smaller. Overall, however, the results are surprisingly invariant. The radon change by moist convection is greatest above 800 mbar in 9L (Figure 12c), associated with its greatest low level convection (Figure 12b). With greater input to the middle troposphere by convection, there is then greater total (large-scale plus eddy) transport to higher levels (Figure 12d). Model 18L convective increases are smallest between 800 and 400 mbar because of its reduced low-level convection. Nevertheless, these differences result in only small changes in radon distribution; for example, in the tropical upper troposphere, radon values vary only from 45 to 53 ($\times 10^{-21}$) in mass mixing ratio amongst the runs.

It was noted previously that large differences existed in the large-scale vertical transport of CFC-11 in the tropics (Figure 3). In fact, differences do exist in vertical transport in specific regions, as precipitation patterns and vertical velocities differ somewhat; the results shown in Figure 3 are due to the use of the new boundary layer in 9L and 18L, which has the effect of altering convergence patterns and reducing the Hadley Cell intensity. However, on the global average the differences are smaller; in fact, while it would appear from Figure 3 that 15L vertical transports are some 33% greater than those in 18L at 400 mbar, on the global average, 18L transports are actually 20% higher. The tropical stream function, indicative of the tropical vertical motion field, is weaker in June–August in 18L, corresponding to somewhat weaker precipitation gradients in the Southern Hemisphere; this then also reduces the associated subsidence and downward transports in the subtropics. Vertical resolution does not play a role here as both 9L and 18L have similar vertical transports, as do 15L and 23L.

6. Interhemispheric Transports

As transport into the stratosphere occurs primarily in the tropics, another factor that could influence tropospheric-stratospheric exchange is the interhemispheric transport. While the primary intent for the CFC-11 and SF_6 tracer experiments was to investigate vertical mixing, differences arose in interhemispheric transport as well. Before leaving these tracers a review of the effects of vertical resolution on this other aspect of model transports will prove useful.

A summary diagnostic of horizontal mixing is the interhemispheric exchange time, defined as the ratio between the hemispheric difference in concentration and (divided by) the cross-equatorial transport. In part I it was noted that the older version of the GISS model had an exchange time of 2.4 years, much longer than the observed value of ~1 year. The 9-layer SIM model had an exchange time of 1.36 years (for CFC-11; the similar diagnostic for ^{85}Kr was 1.27 years).

Interhemispheric exchange times for the runs described here are presented in Tables 4a and 4b. The SIM results for 9 and 18 layers (which did not have the newest boundary layer) are also shown. The new boundary layer (in 9L and 18L) has relatively little effect on the exchange times, and in general, there is little difference amongst the runs. Note that all the models use the same convection scheme; *Gilliland and Hartley* [1997] infer that a change in convection scheme produced slower interhemispheric transport in the Community Climate Model (CCM)3 compared with the CCM2.

One effect that is apparent, however, is that 23L has a significantly faster exchange time than the other models for CFC-11. Model 23L has reduced transport of CFC-11 into the tropical stratosphere; hence more can be advected into the Southern Hemisphere than in the other runs. This distinction is important only for CFC-11, for which transport into the stratosphere represents a sink; 23L is the only model for which the stratospheric sink is actually greater in the Southern Hemisphere than in the Northern Hemisphere (by 5%; in the other models the Northern Hemisphere sink is 1–7% greater). For SF_6, transport into the stratosphere does not represent destruction, and hence interhemispheric transport can occur within the stratosphere in all the runs. Model 9L has a faster exchange time for SF_6 than the other models because of greater southward transport in its thick upper levels, an effect that is mitigated for CFC-11 by the stratospheric sink.

The exchange times are, in general, somewhat faster for SF_6 and, in fact, close to the value calculated by *Geller et al*. [1997] for SF_6 of 1.3 ± 0.1 years. As noted earlier, the SF_6 source was uniform around the latitude band 20°–60°N. To test how the exchange time would vary if the source were put in only over land or on the CFC-11 grid, 9L was rerun with the three different SF_6 source distributions. There was no difference in interhemispheric exchange time between having the source zonally distributed or only over land; both gave values of 1.22 years. When the CFC-11 grid was used, the time went up to 1.32 years, similar to the value found in 9L for CFC-11.

7. Discussion

To summarize the results, shown in Figure 13 are the annual average vertical transport differences in the upper troposphere/lower stratosphere between the other models and the 23L for CFC-11, ^{14}C, and, in addition, potential vorticity, which often acts as a passive tracer. Compared to 23L, the other models produce greater downward transport at 30°–45° latitude; greater upward transports occur equatorward of 30° latitude.

The simulations have shown that 23L produces more realistic transports in terms of the resultant tracer distributions. Comparisons can also be made with mass transports in the atmosphere. *Rosenlof and Holton* [1993] estimated the tropical mass flux through the 100 mbar surface. Shown in Table 5a is a comparison of the different model mass fluxes at their respective levels near that pressure level. Model 23L produces mass fluxes quite close to the observed values for both the annual average and the seasonal variation. Although the observations are somewhat uncertain, this result is consistent with the agreement shown for 23L between modeled and observed tracer distributions. The other models tend to overestimate the tropical mass flux, most egregiously during Northern Hemisphere winter, where the modeled E-P flux convergences in the stratosphere are most obviously too high.

Holton et al. [1995] note that 2-D model transports from the stratosphere into the troposphere tend to occur at high lati-

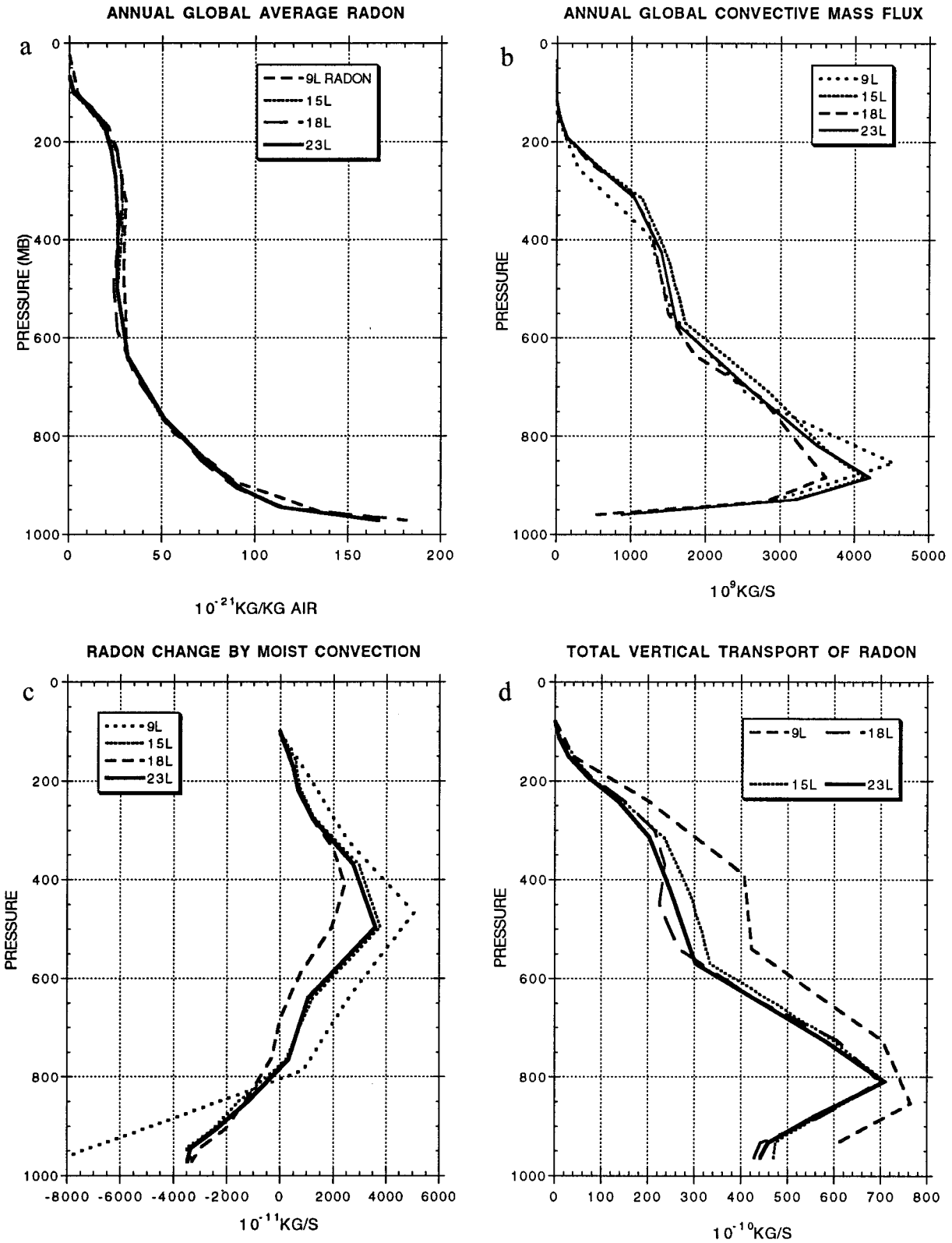

Figure 12. Annual, global average radon distribution as a function of (a) altitude, (b) convective mass flux, (c) radon change by moist convection, and (d) total vertical transport of radon (lower right).

tudes, whereas observations show that they appear to occur in middle latitudes. All the models here feature midlatitude downward transports. This is apparent in the downward fluxes of CFC-11 and ^{14}C (Figures 2 and 11). As noted in section 4, two effects contribute: downward transport by the Eulerian mean circulation, associated with the amplified winter stratospheric residual circulation, and downward transport by upper troposphere-lower stratospheric eddies, also most active in

Table 4a. CFC-11 Interhemispheric Exchange Time

	SIM (9L)	9L	15L	SIM (18L)	18L	23L
Year 2	1.40	1.41	1.47	1.47	1.56	1.17
Year 3	1.33	1.35	1.43	1.40	1.55	1.18
Year 4	1.34	1.43	1.43	1.45	1.57	1.18
Year 5	1.35	1.39	1.37		1.49	1.15
Year 6	1.37	1.35	1.56		1.56	1.15
Average	1.36	1.39	1.45	1.44	1.55	1.17

For the chemical transport model (CTM) the horizontal diffusion coefficient D is at an acceptable range when $D = 1.10–0.70$ [*Prather et al*., 1987].

winter [e.g., *Holton et al*., 1995]. It is probably difficult to accurately parameterize downward transports by eddies, a non–quasi geostrophic feature, in 2-D models.

As emphasized in Figure 13, the values are notably higher in the other models than in 23L, especially during Northern Hemisphere winter (Figure 11). As the residual circulation is itself driven by eddy fluxes, the reduced eddy energy in 23L minimizes the total downward transport in midlatitudes compared with the that of the other models.

Shown in Table 5b is a comparison of the model's downward mass flux in the extratropics with the observations of *Rosenlof and Holton* [1993]. The extratropics are defined as poleward of 15° latitude, as given by *Rosenlof and Holton* [1993] for the winter season. Only 23L does not strongly overestimate the downward mass flux. Also shown in Table 5b are estimated mass fluxes of *Eluszkiewicz et al*. [1997] using UARS data to calculate the thermodynamic energy equation (the range of values comes from estimating the temperature change with time term from either Microwave Limb Sounder (MLS) (the smaller number) or cryogenic limb array etalon spectrometer (CLAES) data). Northern Hemisphere winter results are in relatively good agreement with both 23L and previous observations. However, as noted by *Eluszkiewicz et al*. [1997], the Southern Hemisphere winter values in this reconstruction are more similar to Northern Hemisphere values than those in the *Rosenlof and Holton* [1993] estimation, a perspective also not shared by any of the GCM results. The *Eluszkiewicz et al*. [1997] definition of the extratropics actually started at a somewhat higher latitude (25°–30°), where downward vertical velocities first appeared in their data reconstruction. Applying that correction to the model only increased the Southern Hemisphere downward flux by ~5%.

There is some reason to believe that the winter downward flux should be larger in the Northern Hemisphere. In each of the GCM runs the colder tropical tropopause temperature occurred during Northern Hemisphere winter (e.g., in 18L it was −83°C at 2°N in December–January, −81°C in June through August; in 23L the temperatures were 2°C warmer in each season). This seasonal variation matches observations for both tropical tropopause temperatures and water vapor [e.g., *Rind et al*., 1993]. It is apparently associated with the stronger stratospheric residual circulation during Northern Hemisphere winter, an effect which occurs in the model; for example, in 23L the Northern Hemisphere residual circulation from 100 to 10 mbar during December–February is ~20% stronger than its Southern Hemisphere counterpart in June–August. The origin of this difference is believed to be associated with the greater stationary wave forcing; in 23L, winter stationary wave energy between 150 and 10 mbar is 2.7 times larger in the Northern Hemisphere, and total eddy energy is 24% greater. E-P flux convergences in the same region are 45% larger. (In contrast, gravity wave drag is 10% larger in the Southern Hemisphere, dominated by the nonorographic component acting on stronger winds.)

The large downward mass fluxes in most of the models result from an apparent overestimate of the residual circulation in the stratosphere driven by excess E-P flux convergences and gravity wave drag near the model top. This excess is produced by large eddy energy in the upper troposphere, perhaps produced by too low a stability in the upper troposphere/lower stratosphere, and the position of the model top at 10 mbar, guaranteeing E-P flux convergences and strong drag below that level. Model 18L is considerably worse than the other models for it has the vertical resolution in the upper troposphere to generate large eddy energy values, it lacks gravity wave drag in the lower stratosphere and thus has reduced stability, allowing for more easy generation of eddy energy, and it has its top at 10 mbar. Model 15L has lower stratospheric gravity wave drag and reduced eddy energy, but with the top at 10 mbar it still produces too large an E-P flux convergence. Model 9L has reduced resolution with less eddy energy production and a specified drag in a thick top layer so that the stability is not as bad as in 18L, but it still has a top at 10 mbar.

Moving the top of the model to the stratopause region, as is done for many of the newer models participating in the AMIP II intercomparisons, has some positive effects compared to the models with lower tops but does not solve the transport problems. The stability in the lower stratosphere is improved compared with the models with middle stratosphere tops and is only slightly worse than models with the top at the mesopause. Large E-P flux convergences arise near the stratopause now and help drive an amplified residual circulation, although, again, the values are more realistic in the lower stratosphere than in the models with the lower top. The transport of ^{14}C from the "overworld" above 100 mbar (or the 380 K surface) is negatively affected relative to the models with the higher tops but, again, is better than the model with the lower top; note that reduced upper tropospheric eddy energy does occur in 23LT compared to 15LT (Table 1), which affects the eddy contribution to downward fluxes. However, as shown by the SF_6 results, upward transport through 100 mbar in the tropics is no better than in 15L with its 10 mbar top. To compensate for the strong winds induced by the location of the top, the gravity wave drag in the upper stratosphere region is much stronger than would occur there (in 23L) without the top (Table 1). This imparts a meridional circulation that on the annual average, flows away from the equator in each hemisphere, with upward flow in the tropical stratosphere over a depth that extends down to the tropopause; the tropical mass flux through 100 mbar is 75% greater in 23LT than in 23L (consistent with the SF_6 fluxes). The same qualitative effect occurs when the model top is lower except that the winds at 10

Table 4b. SF-6 Interhemispheric Exchange Time

	9L	15L	18L	23L
Year 2	1.21	1.36	1.33	1.26
Year 3	1.16	1.34	1.30	1.25
Year 4	1.19	1.35	1.30	1.23
Year 5	1.14	1.33	1.26	1.27
Year 6	1.16	1.35	1.24	1.23
Average	1.17	1.35	1.29	1.25

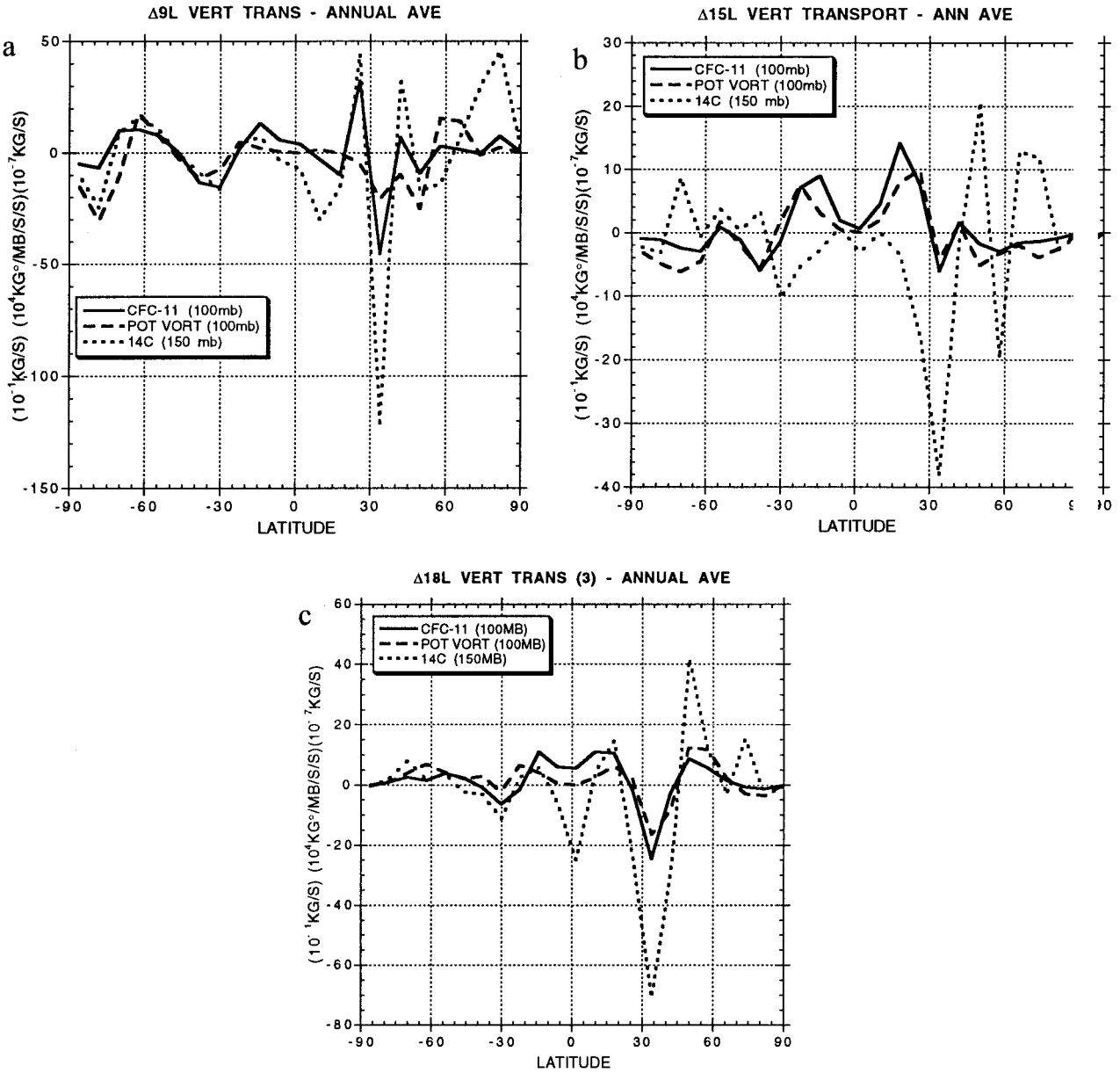

Figure 13. Difference between (a) 9L, (b) 15L, and (c) 18L from 23L for the annual average vertical transports of CFC-11 and potential vorticity through the 100 mbar level and ^{14}C through 150 mbar.

mbar are normally weaker; hence the meridional circulation effect is much more muted. Putting the top near the stratopause maximizes this spurious circulation because of the maximum winds normally found there.

It may seem paradoxical that the models with the most energy and most downward transport at high latitudes in the lower stratosphere are also coldest in the lower stratosphere (Figure 5). While it is true that the large-scale subsidence associated with the residual circulation is providing a warming tendency in these models, of more importance is their reduced northward heat transport by planetary waves, despite their

Table 5a. Tropical Upward Mass Fluxes (15°N–15°S)

	DJF	JJA	Annual Mean
Observed (100 mbar)	114	56	85
9L (150 mbar)	176	55	129
15L (124 mbar)	132	92	118
18L (113 mbar)	173	93	115
23L (117 mbar)	108	53	83

Fluxes are in 10^8 kg s^{-1}; DJF is December, January, and February; JJA is June, July, and August.

Table 5b. Winter Extratropical Downward Mass Fluxes (10^8 kg s^{-1})

	NH (Dec–Feb)	SH (June–Aug)
Observed (100 mbar)	125 (R&H); 87–112 (E)	58 (R&H); 104–108 (E)
9L (150 mbar)	216	139
15L (124 mbar)	154	128
18L (113 mbar)	176	136
23L (117 mbar)	102	72

NH is Northern Hemisphere; SH is Southern Hemisphere.

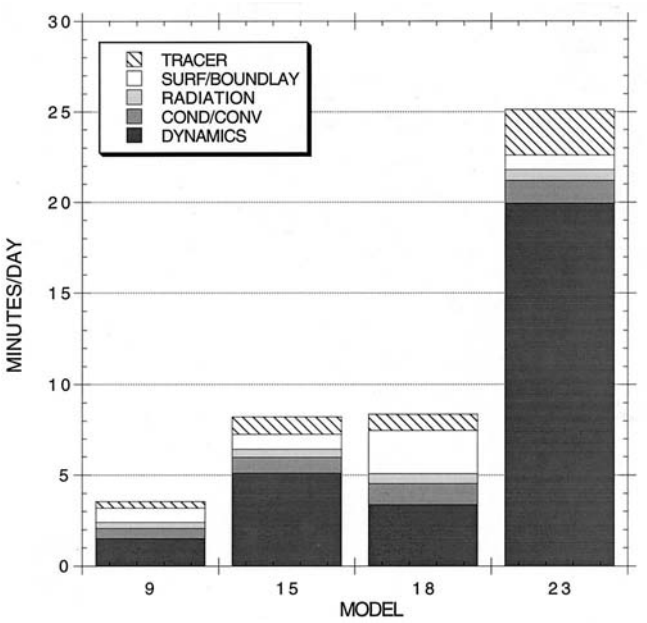

Figure 14. Timing for different model resolutions/processes on the SGI 2000.

greater planetary wave energy. For waves to transport heat poleward in a west wind regime the planetary wave energy has to be propagating vertically, and the existence of the model top in the middle stratosphere is apparently sufficient to reduce eddy propagation and poleward heat transport.

Therefore producing proper transport between the troposphere and stratosphere from the GISS modeling perspective requires increased vertical resolution, gravity wave drag, and the top of the model to be considerably above the stratosphere. To appreciate the impact these features have on the models when run on IBM or SGI workstations, we present in Figure 14 the timing used by the various subroutines. The times are specifically for one processor of an SGI Origin 2000 workstation.

A number of the elements in Figure 14 require explanation. The time taken by the dynamical subroutine depends on more than just the number of layers, which provides a linear factor. When higher layers of the atmosphere are included, the dynamical time step must be shortened for the stronger winds create potential numerical instability conditions. Gravity wave drag, included in the dynamics, adds ~20% to the model run time. The boundary layer in 9L and 18L takes a higher proportion of the running time because of the use of the second-order closure scheme. The radiation routine appears to take only a small percentage of the total time because the full radiation, including the effect of cloud cover changes, is called only once every 5 hours (although solar radiation and temperature changes are updated each hour). Hence its time should be increased by close to a factor of 5 for comparison with other GCMs. Each tracer adds ~10% to the total running time including that tracer.

Comparison between the best model L23 and the worst L18 provides a sobering perspective. To provide better tropospheric-stratospheric exchange, with an addition of only 5 layers overall and none in the region of the upper troposphere/lower stratosphere, requires a model running time increase of a factor of 3.

8. Conclusions

On-line tracers are used to explore the necessary vertical resolution and associated processes in GCM model development. Results for transport from the troposphere into the stratosphere, or stratosphere down into the troposphere, show that the primary factor of importance is the intensity of the residual circulation within the stratosphere, at least in the models tested here. Increasing the vertical resolution near the tropopause does not by itself improve tropospheric-stratospheric exchange; lifting the top of the model out of the stratosphere appears to be a requirement, as well as including gravity wave drag in the lower stratosphere. None of the models utilized in the AMIP intercomparisons has a model top sufficiently high to qualify if our results can be generalized for other GCMs.

A number of other transport features that could affect tropospheric-stratospheric exchange are surprisingly insensitive to vertical resolution. These include vertical mixing within the troposphere and interhemispheric transport. An exception to this last conclusion is when tropospheric-stratospheric exchange itself affects interhemispheric transport, as in the case of CFC-11, with destruction in the stratosphere. The use of a new boundary layer scheme produces differences in large-scale vertical transport in the tropics by altering the precipitation field without having a noticeable impact on interhemispheric or stratospheric-tropospheric exchange.

Decisions concerning the proper vertical resolution to use in a GCM are made on a variety of grounds, including having the proper resolution to input radiative perturbations (volcanic aerosols and ozone changes) or chemical perturbations (such as aircraft releases). Producing the proper absolute temperature of the tropical tropopause is a necessity for simulating stratospheric water vapor [e.g., *Rind et al*., 1988], and the results shown here emphasize that insufficient stability in the upper troposphere/lower stratosphere results in excessive vertical mixing between the two regions. For the purposes of tropospheric-stratospheric exchange, emphasis must be given to simulating the stratosphere properly, as well as the troposphere, when deciding on model vertical structure, although inclusion of high levels of the atmosphere substantially increases model computational time.

Even though these models use higher-order schemes for heat and momentum transport (part I), it is likely that their relatively coarse horizontal resolution would not be able to produce overly realistic tropopause folds, overshooting convective plumes, and other small-scale features that may govern actual transport into and out of the troposphere in the real world. The model seems to provide analogs to these phenomena that allow 23L to produce realistic stratospheric-tropospheric exchange rates. Utilizing finer horizontal resolution would help in producing these features more realistically. Finer horizontal resolution also would seem to require an increase in vertical resolution to resolve the smaller-scale eddies, although the precise relationship between the two resolutions has not been resolved within the modeling community. Future model studies should incorporate changes in both resolutions to investigate these issues further.

Acknowledgments. This work was supported by the NASA Atmospheric Chemistry and Modeling Program (ACMAP) and a NASA EOS/IDS grant for including on-line chemistry in the GISS GCM. KS was supported by NSF grant ATM-96-28843. Climate model development at GISS is supported by the NASA Climate Modeling Program.

References

Boer, G. J., and M. Lazare, Some results concerning the effect of horizontal resolution and gravity wave drag on simulated climate, *J. Clim*., *1*, 789–806, 1988.

Boering, K. A., B. C. Dange, S. C. Wofsey, M. Loewenstein, J. R. Podolske, and E. R. Kein, Tracer-tracer relationships and lower stratospheric dynamics: CO_2 and N_2O correlations during SPADE, *Geophys. Res. Lett*., *21*, 2567–2570, 1994.

Boville, B. A., Sensitivity of the simulated climate to model resolution, *J. Clim*., *4*, 469–485, 1991.

Boyle, J. S., Sensitivity of dynamical quantities to horizontal resolution for a climate simulation using the ECMWF (cycle 33) model, *J. Clim*., *6*, 796–815, 1993.

Del Genio, A. D., and M.-S. Yao, Efficient cumulus parameterization for long-term climate studies: The GISS scheme, in *The Representation of Cumulus Convection in Numerical Models*, *Meteorol. Monogr*., vol. 46, edited by K. Emanuel and D. Raymond, pp. 181–184, Am. Meteorol. Soc., Boston, Mass., 1992.

Del Genio, A. D., M.-S. Yao, W. Kovari, and K.-W. Lo, A prognostic cloud water parameterization for global climate models, *J. Clim*., *9*, 270–304, 1995.

Eluszkiewicz, J., D. Crisp, R. G. Grainger, A. Lambert, A. E. Roche, J. B. Kumer, and J. L. Mergenthaler, Sensitivity of the residual circulation diagnosed from the UARS data to the uncertainties in the input fields and to the inclusion of aerosols, *J. Atmos. Sci*., *54*, 1739–1757, 1997.

Galperin, B., L. H. Kantha, S. Hassid, and A. Rosati, A quasi-equilibrium turbulent energy model for geophysical flows, *J. Atmos. Sci*., *45*, 55–62, 1988.

Geller, L. S., J. W. Elkins, J. M. Lobert, A. D. Clarke, D. F. Hurst, J. H. Butler, and R. C. Myers, Tropospheric SF_6: Observed latitudinal distribution and trends, derived emissions, and interhemispheric exchange time, *Geophys. Res. Lett*., *24*, 675–678, 1997.

Gilliland, A. B., and D. E. Hartley, Interhemispheric transport and the role of convective parameterizations, *J. Geophys. Res*., *103*, 22,039–22,045, 1998.

Hall, T. M., and R. A. Plumb, Age as a diagnostic of stratospheric transport, *J. Geophys. Res*., *99*, 1059–1070, 1994.

Hansen, J., G. Russell, D. Rind, P. Stone, A. Lacis, S. Lebedeff, R. Ruedy, and L. Travis, Efficient three dimensional global models for climate studies: Models I and II, *Mon. Weather Rev*., *111*, 609–662, 1983.

Hartke, G., and D. Rind, Improved surface and boundary layer models for the GISS GCM, *J. Geophys. Res*., *102*, 16,407–16,422, 1997.

Haynes, P. H., C. J. Marks, M. E. McIntyre, T. G. Shepherd, and K. P. Shine, On the "downward control" of extratropical diabatic circulations by eddy-induced mean zonal forces, *J. Atmos. Sci*., *48*, 651–678, 1991.

Hoke, J. E., Improving the horizontal resolution of the nested grid model, *Tech. Proc. Bull. 368*, 9 pp., *Natl. Weather Serv*., Washington, D. C., 1987. (Available from the U.S. Dep. of Commer., Washington, D. C.)

Holton, J. R., P. H. Haynes, M. E. McIntyre, A. R. Douglass, R. Rood, and L. Pfister, Stratosphere-troposphere exchange, *Rev. Geophys*., *33*, 403–439, 1995.

Intergovernmental Panel on Climate Change (IPCC), *Climate Change 1992*, edited by J. T. Houghton, B. A. Callander, and S. K. Varney, 93 pp., Cambridge Univ. Press, New York, 1992.

Johnston, H. S., Evaluation of excess carbon-14 and strontium-90 for suitability to test two-dimensional stratospheric models, *J. Geophys. Res*., *94*, 18,485–18,493, 1989.

Jones, P. W., K. Hamilton, and R. J. Wilson, A very high resolution general circulation model simulation of the global circulation in austral winter, *J. Atmos. Sci*., *54*, 1107–1116, 1997.

Kaye, J. A., S. A. Penkett, and F. M. Ormond (Eds.), Report on concentrations, lifetimes and trends of CFCs, halons, and related species, *NASA Ref. Publ*., *1339*, 169, 1994.

McCormick, M. P., E. W. Chiou, L. R. McMasters, W. P. Chu, J. C. Larsen, D. Rind, and S. Oltmans, Annual variations of water vapor in the stratosphere and upper troposphere observed by the Stratospheric Aerosol and Gas Experiment II, *J. Geophys. Res*., *98*, 4867–4874, 1993.

Mote, P. M., K. H. Rosenlof, J. R. Holton, R. S. Harwood, and J. W. Walters, Seasonal variations of water vapor in the tropical lower stratosphere, *Geophys. Res. Lett*., *22*, 1093–1096, 1995.

Oort, A. H., Global atmospheric circulation statistics, 1958–1973, *NOAA Prof. Pap. 14*, 180 pp., U.S. Dep. of Comm., Washington, D. C., 1983.

Patra, P. K., S. Lal, B. H. Subbaraya, C. H. Jackman, and P. Rajaratnam, Observed vertical profile of sulphur hexafluoride (SF_6) and its atmospheric applications, *J. Geophys. Res*., *102*, 8855–8859, 1997.

Phillips, T. J., A summary documentation of the AMIP models, *PCMDI Rep. 18*, 343 pp., Lawrence Livermore Natl. Lab., Livermore, Calif., 1994.

Prather, M., Numerical advection by conservation of second-order moments, *J. Geophys. Res*., *91*, 6671–6681, 1986.

Prather, M., Special Numerical Experiment, Simulation of $CFCl_3$ as a test for 3-D atmospheric models, in *Report for WCRP Workshop on Long-Range Transport of Trace Gases 10–14 December 1990*, World Meteorol. Org., Geneva, 1992.

Prather, M. J., and E. E. Remsberg (Eds.), *The Atmospheric Effects of Stratospheric Aircraft*: *Report of the 1992 Models and Measurements Workshop*, vol. III, *Special Diagnostic Studies*, *NASA Ref. Publ*., *1292*, *III*, 352, 1993.

Rind, D., Dependence of warm and cold climate depiction on climate model resolution, *J. Clim*., *1*, 965–997, 1988.

Rind, D., and J. Lerner, Use of on-line tracers as a diagnostic tool in general circulation model development, *J. Geophys. Res*., *101*, 12,667–12,683, 1996.

Rind, D., R. Suozzo, N. K. Balachandran, A. Lacis, and G. L. Russell, The GISS Global Climate/Middle Atmosphere Model Part I: Model structure and climatology, *J. Atmos. Sci*., *45*, 329–370, 1988.

Rind, D., E.-W. Chiou, W. Chu, J. Larsen, S. Oltmans, J. Lerner, M. P. McCormick, and L. McMasters, Overview of the SAGE II water vapor observations: Method, validation, and data characteristics, *J. Geophys. Res*., *98*, 4835–4856, 1993.

Rosenloff, K. H., and J. R. Holton, Estimates of the stratospheric residual circulation using the downward control principle, *J. Geophys. Res*., *98*, 10,465–10,479, 1993.

Rosenzweig, C., and F. Abramopoulos, Land-surface model development for the GISS GCM, *J. Clim*., *10*, 2040–2054, 1997.

Shah, K., and D. Rind, Use of microwave brightness temperatures with a GCM, *J. Geophys. Res*., *100*, 13,841–13,874, 1995.

Shah, K., and D. Rind, Comparing upper tropospheric and lower stratospheric temperatures: Microwave sounding unit, radiosonde, COSPAR International Reference Atmosphere, and National Center for Environmental Prediction/National Center for Atmospheric Research reanalysis monthly mean climatologies, *J. Geophys. Res*., *103*, 31,569–31,591, 1998.

Volk, C. M., et al., Evaluation of source gas lifetimes from stratospheric observations, *J. Geophys. Res*., *102*, 25,543–25,564, 1997.

Waugh, D. W., et al., Three-dimensional simulations of long-lived tracers using winds from MACCM2, *J. Geophys. Res*., *102*, 21,493–21,430, 1997.

Wu, M. F., M. A. Geller, E. R. Nash, and M. E. Gelman, Global atmospheric circulation statistics: Four year averages, *NASA Tech. Mem*., *100690*, 69, 1987.

J. Lerner, Science Systems and Applications, New York, NY 10025.

D. Rind, Goddard Institute for Space Studies, Goddard Space Flight Center, New York, NY 10025. (drind@giss.nasa.gov)

K. Shah and R. Suozzo, Center for Climate Systems Research, Columbia University, New York, 10025.

(Received January 31, 1998; revised September 14, 1998; accepted December 23, 1998.)